Oil absorption stability of modified cellulose porous materials with super compressive strength in the complex environment

Daning Lang · Chengbo Zhang · Qianqian Qian · Chengxin Guo · Lingling Wang · Chao Yang · Ronglan Wu · Wei Wang · Jide Wang · Jihong Fu

Abstract The occurrence of oil spills has severe damage upon both the environment and human health. Hence, the development of a green, recyclable, complex environment resistant, and efficient oil–water separation aerogel is required in order to effectively absorb marine or industrial oil. In this study, modified cellulose/N,N'-methylenebisacrylamide/tannin (PCMT) composite porous materials were prepared utilizing the sol–gel method and were modified with tertbutyl acrylate. PCMT possesses a three-dimensional interpenetrating porous structure, exhibiting remarkable oil–water separation performance and excellent compressive strength (PCMT can capable of bearing 7000 times its own weight; PCMT can endure 290.3 kPa pressure at 80% strain when the amount of tannin is 0.2 g). The unique pore structure of PCMT engenders differential oil adsorption capacities (PCMT0, PCMT0.05, PCMT0.1, and PCMT0.2 evince higher adsorption capacities for petroleum ether and dichloromethane, n-hexane and dichloromethane, toluene, and toluene and dichloromethane, respectively). Of critical import, PCMT demonstrates exceptional adaptability to complex environments, wherein the porous materials maintain good hydrophobicity and oil absorption capacity under conditions of vigorous stirring, a wide pH range (1–14), a wide temperature range (4–160 °C), ultraviolet irradiation (8 h), and tape peeling (10 times). Moreover, the porous materials may be employed for the recovery of oil through simple mechanical extrusion, thus demonstrating certain economic significance and the application potential in the treatment of oil spills.

Keywords Cellulose · Porous material · Surface coating · Hydrophobicity · Oil absorption

D. Lang · C. Zhang · Q. Qian · C. Guo · L. Wang · C. Yang · R. Wu (✉) · J. Wang · J. Fu
Key Laboratory of Oil and Gas Fine Chemicals, School of Chemical Engineering, Xinjiang University, Urumqi 830046, China
e-mail: wuronglan@163.com

W. Wang (✉)
Institute of Chemistry, University of Bergen, 5007 Bergen, Norway
e-mail: wei.wang@uib.no

W. Wang
Center for Pharmacy, University of Bergen, 5020 Bergen, Norway

Introduction

The usage of oil-absorbing materials is wide-ranging in both the domains of environmental science and industrial production, as evidenced by various studies (Liu et al. 2019; Tai et al. 2022; Zhang et al. 2021). Porous materials that feature

an interconnected network structure with low relative density, high specific strength, and good permeability are extensively employed for oil absorption purposes (Qin et al. 2019; Zhang et al. 2022). Modified cellulose adsorptive materials offer several advantages, such as being low cost (Peng et al. 2020), lightweight (Wu et al. 2021), highly absorptive (Liu et al. 2016, 2018), highly hydrophobic (Hammouda et al. 2021; He et al. 2018), and possessing high mechanical strength (Cheng et al. 2020) in comparison to materials such as graphene (Cao et al. 2018; Dai et al. 2020) and carbon nanotubes (Nie et al. 2019). However, these properties are insufficient for the treatment of oily sewage in industrial or oceanic pollution due to the poor compressive strength and environmental adaptability of most cellulosic materials. The majority of industrial oily wastewater is either acidic or alkaline, while oily sewage at sea is exposed to a harsh environment. Thus, it is necessary to develop cellulose absorbent materials with good adaptability to complex environments such as high temperature, wind and wave, ultraviolet radiation, strong acid and strong alkali, and others to deal with industrial and marine oily wastewater.

The resistance of materials in complex environments is contingent on their intrinsic properties or on the properties of the modifiers that are incorporated during the preparation of cellulose-based materials. Consequently, it is of importance to find agents and materials that exhibit excellent physical and chemical stability, including resistance to water, acids, alkalis, and high temperatures. In the realm of oil-absorbing materials, the wetting properties are a function of both the surface morphology and chemical composition of the materials. Through a chemical reaction or a physical composite of functional groups, the surface energy of the materials can be reduced by introducing hydrophobic components. For example, siloxane reagents, long-chain alkanes, and fluorine-containing compounds have been shown to improve the hydrophilicity of cellulose and cellulose-based materials. Moreover, the incorporation of nanoparticles can modulate the microstructure of materials, which can in turn enhance the adsorption selectivity of hydrophobic organic reagents on cellulose-based materials. These findings have been documented in various studies (Chen et al. 2019;

Cho et al. 2017; Fu et al. 2018; Lorevice et al. 2020; Patowary et al. 2016; Zhang et al. 2022).

Low surface energy materials often exhibit robust resistance to acid and alkali (Liu et al. 2018; Wang and Liu 2019; Zhang 2020). However, the chemical reactions of functional groups can diminish cellulose's hydrogen bonding and crystalline structure, thereby impeding the mechanical properties and degradability of the resulting porous materials. Additionally, the physical combination of cellulose and a modifier is indeed challenging. Hence, researchers first made cellulose porous materials and subsequently rendered them oil-absorbent through physical compositing, hydrophobic modification via vapor deposition, or impregnation coating (Fei et al. 2022). Das and De (2015) utilized the sol–gel method to synthesize fluoroalkyl-functionalized zirconia, which then facilitated the development of remarkably durable superhydrophobic coatings on cotton fabrics through a simple dipping technique. The resulting coating showed an extraordinarily improved water contact angle ($163° \pm 1°$), coupled with superlipophilicity, and enduring waterproofing capabilities in the face of challenging environmental conditions, such as high temperature, and strongly acidic or alkaline solutions. Despite cellulose's superior temperature resistance and chemical corrosion stability, few porous materials have been documented to bear outstanding oil absorption stability in harsh environments (e.g., high temperatures, broad pH range, ultraviolet irradiation). Hydrophobic modifiers currently in existence are somewhat limited and not optimally suited for deployment in intricate settings. Thus, it is vital to develop cellulose-absorptive materials capable of withstanding complicated environmental factors while simultaneously exhibiting superior oil–water separation performance and stability.

Tertbutyl acrylate (TBA) is an organic acid ester. Its unique carbon–carbon double bond and tertbutyl structure permit grafting and polymerization (Davis and Matyjaszewski 2000; Klein et al. 1991). Additionally, TBA displays excellent resistance to aqueous and chemical corrosion, thereby rendering it suitable for an extensive array of applications, encompassing coatings, detergents, leather, adhesives, and other domains. Wu et al. (2019) undertook the modification of photonic crystals (PCs) with hydrophobic tertbutyl acrylate (p(TBA)) and, in so doing, accomplished the production of p(TBA) PCs

thin film material possessing superlative hydrophobic properties. Hai et al. (2018) synthesized Nitraria seeds meal-g-poly(methyl methacrylate-co-tert-butyl acrylate) resin through graft copolymerization and subsequently attained a resin of admirable oil absorption efficacy. Notably, the resin evinced excellent hydrophobicity, lipophilicity, and network structure in a 0.9 wt% NaCl solution. Its capacity for rapeseed oil, diesel oil, and gasoline absorption attained magnitudes of 24.3, 22.7, and 21 times its weight, correspondingly.

In an effort to address the issues concerning stability of oil absorption, mechanical robustness, and environmental resilience of oil-absorbing materials in the separation of oil-containing wastewater in industrial and marine settings, we have develop a universal hydrophobic modifier for cellulose-g-TBA polymer (PTBA), in light of the exceptional properties of TBA and the remarkable strength of cellulose. Through the sol–gel method, we synthesized porous cellulose/N,N'-methylenebisacrylamide/tannin composites (PCMT), utilizing cellulose as the active matrix, N,N'-methylenebisacrylamide (MBA) as a crosslinking agent, and tannin as an additive with slow penetration speed. The internal pore structure of the materials was regulated by modifying the amount of tannin, in order to reduce the crosslinking polymerization of cellulose and MBA, based on the unique three-dimensional network structure of cellulose porous materials. Subsequently, we utilized surface coating technology to subject the porous materials (PCMT) to hydrophobic modification. The resulting PCMT exhibited impressive compression resistance, superior oil–water separation capacity, and notable adaptability to the environment.

Materials and methods

Materials

Cellulose (50 mm) was purchased from Hebei Balinway Superfine Materials Co., Ltd.; 1-allyl-methylimidazolium chloride (AMIMCl, 99%) from Moni Mooney Chemicals Co., Ltd; 2-bromo-2-methylpropionyl bromide (97%); Ethyleneglycol dimethacrylate (EGDMA, 98%), N,N,N',N'',N''-pentamethyldiethylenetriamine (PMDETA, 98% purity) and Tert-butyl acrylates (TBA, 99%) from

Aladdin Reagent Co., Ltd.; Cuprous (I) bromide (CuBr, 98%) from Across Chemical Co., Ltd; N,N'-Methylenebisacrylamide (MBA, 98%) Tianjin Institute of Chemical Reagent; Tannin, Urea (99%), Sodium hydroxide (NaOH, 96%) and other reagents were purchased from Tianjin Hongyan Reagent Factory; Nitrogen (99.99%) was purchased separately from Xinjiang Xintianyi Co., Ltd. All the water used in the experiment was deionized water.

Preparation of cellulose/MBA/tannin (CMT) composite materials

Cellulose (5 g) was dispersed in a mixed solution (100 g) of NaOH/urea/H_2O (7/12/81, weight ratio) and stirred with a rotating speed of 800 r/min for 20 min to sufficiently distribute the cellulose. The cellulose dispersion was stored in a freezer at -20 °C overnight. Then, it was taken out and thawed at room temperature to obtain a light yellow and completely dissolved cellulose solution (5 wt%). Then MBA (0.4 g) was added to the cellulose solution (25 g), stirring for 5 h at room temperature. After MBA was dissolved entirely, tannin (0, 0.05, 0.1, 0.2 g) was added to the solution and stirred for 1 h. The solution was poured into a mold having a diameter of 1 cm and a height of 0.7 cm. It stood still for 6 h at room temperature, and then hydrogels were formed (see Scheme 1a). The hydrogels were immersed in deionized water for dialysis until the dialysis media was neutral in pH. Dialysis media was changed four times daily, and the dialysis took 3 days. Then the hydrogels were frozen at -20 °C completely. Finally, the diameter was about 15 mm, and the height about 10 mm of porous materials was obtained by freeze-drying for 48 h at -54 °C. The porous materials were named CMT. For example, when 0.05 g tannin was used during the synthesis, CMT0.05 was used for the sample. At the same time, the cellulose solution of 2 wt%, 3 wt% and 4 wt% were also tried during preliminary experiments. However, hydrogel formed only with 5 wt% cellulose solution. Therefore, the cellulose solution of 5 wt% was used in the following experiments.

Scheme 1 **a** Schematic diagram of the hydrogels forming process; **b** Schematic showing the experimental process of the PCMT
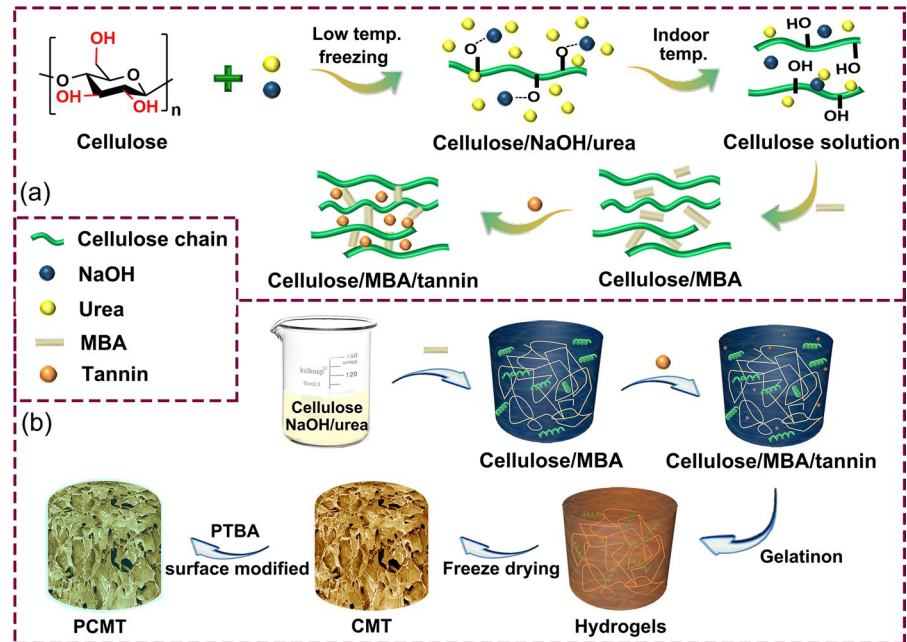
Preparation of tert-butyl acrylate modified cellulose/ MBA/tannin (PCMT) composites

Cellulose-Br was synthesized based on a method reported in our previous work (Lang et al. 2021). CuBr (7.5 mg), PMDETA (43.3 mg) and ascorbic acid (9.5 mg) were dissolved in DMF (100 mL). Cellulose-Br (0.5 g) was added to 37.5 mL of the DMF solution. After it was fully dissolved, TBA (20 mL) was added. Then the flask was sealed with a rubber stopper and purged with nitrogen for 30 min. Then, the flask was polymerized in a water bath at 60 °C for 24 h, and the TBA-g-cellulose (PTBA) was obtained. The PCMT were obtained by soaking cellulose porous materials (CMT) in PTBA solution for 1 min and then taken out, then drying it in an oven at 70 °C for 2 h (Scheme 1b).

Density and porosity of CMT

The apparent density (ρ, g/cm^3) of the sample was calculated by Eq. (1).

$$\rho = \frac{m}{V} \tag{1}$$

where m (g) and V (cm^3) are the weight and volume of the samples. According to the solid density and weight ratio of each component of the samples, and the density (ρ_s, g/cm^3) and porosity (P, %) of CMT

were calculated according to Eqs. (2) and (3) (Yin et al. 2017):

$$\rho_s = \left(\frac{W_{cellulose}}{\rho_{cellulose}} + \frac{W_{MBA}}{\rho_{MBA}} + \frac{W_{tannin}}{\rho_{tannin}} \right)^{-1} \tag{2}$$

$$P(\%) = \left(1 - \frac{\rho}{\rho_s} \right) \times 100\% \tag{3}$$

where W, ρ (g/cm^3) and P (%) are the weight fraction, solid density and porosity percentage of the materials. The values $\rho_{Cellulose}$, ρ_{MBA} and ρ_{Tannin} are 1.5, 1.235 and 2.12 g/cm^3, respectively.

Oil absorption test of PCMT

The oil–water mixtures were prepared with 10 mL of deionized water dyed methylene blue with 10 mL of oil dyed oil red (taking n-hexane as an example). PCMT adsorbed oil in the oil–water mixtures for a certain period (2 s∼1 min), and the quality of PCMT before and after absorption was recorded. The absorbing capacity (Q) of oil was calculated by Eq. (4) (Wang and Liu 2019).

$$Q = \frac{m_2 - m_1}{m_1} \qquad (4)$$

where Q (g/g) is the absorptive capacity, and m_1 (g) and m_2 (g) are the total mass of the PCMT before and after oil absorption, respectively. The Q values in this paper were the absorbed amount of oil in 1 min. Because the absorption rates for the four porous materials (PCMT) were different, and the adsorption saturation could be achieved in 1 min, the absorptive capacity at the absorption time of 1 min was selected to evaluate the oil absorptive capacity of the four porous materials. All experiments and data are obtained from three experiments.

Cyclic testing of PCMT

The PCMT were placed in oil/water mixtures in one cycle first. After the absorption reached saturation, the PCMT were taken out. The absorbed oil in PCMT was removed by manual extrusion. The cycle test was stopped until the PCMT could not absorb oil from oil/water mixtures or the absorption capacities decreased significantly. The mass of the PCMT were recorded after each absorption saturation and after extrusion, calculate the oil absorption of the porous materials during the cycle according to Eq. (4).

Characterization

The bond properties were characterized by Fourier transform infrared spectroscopy (FTIR; VERTEX 70, Bruker, Germany) using KBr disk, where the spectra were recorded within the wavenumber of 500–4000 cm^{-1}. The morphology of PCMT were observed by scanning electron microscopy (SEM; TM303, Hitachi, Japan). The thermal stabilities of the materials were evaluated by thermal gravimetric analysis (TG; SDT Q600, TA, America) in the temperature range of 25–800 °C with the increase rate of 10 °C/min, and the samples were in N_2 atmosphere. The oleophobic properties of CMT and PCMT surfaces were characterized by contact angle measurements (JJ2000B, Zhongchen, Shanghai, China) at room temperature. Static mechanical test (Tinius Olsen, H5K-T, USA) was measured for the compressive resistance of porous materials. The compression speed was 50 mm/min at 25 °C, the sample had a cylindrical shape (diameter was about 15 mm and high were about 10 mm), the test temperature was room temperature (25 °C), the humidity was 25–30%, and the sample was immersed entirely in n-hexane.

Results and discussion

Gelation of CMT hydrogels

The gelation of CMT was examined through the inversion of the sample tubes (as depicted in Fig. 1a). The gelation process was found to require increased time with greater tannin content. Notably, it took approximately 3 h for CMT0 to achieve complete formation, while other samples required less than 6 h to form a gel. This prolonged gelation time is a result of tannin acting as a competitor to cellulose, possessing multiple hydroxyl groups in both molecules. Moreover, the presence of tannin increases the distance between cellulose and MBA, thereby inhibiting the formation of hydrogen bonds between them. Upon removal from the mold, the hydrogels were observed to remain intact and elastic, as shown in Fig. 1b. Additionally, the gels were capable of regaining their original shape in a noticeably brief period of time after compression. The color of the CMT hydrogels became lighter after washing and soaking (as indicated in the first step of Fig. 1c), implying that tannin had been removed from the hydrogel during dialysis. It is plausible to consider tannin as a soft template for the preparation of porous materials (as depicted in Fig. 1c). Notably, no collapse was observed during the freeze-drying process of the hydrogels. With the exception of color, no macroscopic differences were observed among the CMT samples.

Morphology and structure analysis of cellulose porous materials

The micro-morphology of the porous materials was subjected to a comprehensive investigation, employing Scanning Electron Microscopy (SEM), as depicted in Fig. 2. The CMT is characterized by an intricate porous architecture, as evidenced by the images in Fig. 2a–d. Conversely, the surface of these materials exhibits a conspicuously smooth texture, as apparent from Fig. 2e–h. For instance, upon analyzing PCMT0.1 (Fig. 2m), its internal architecture was
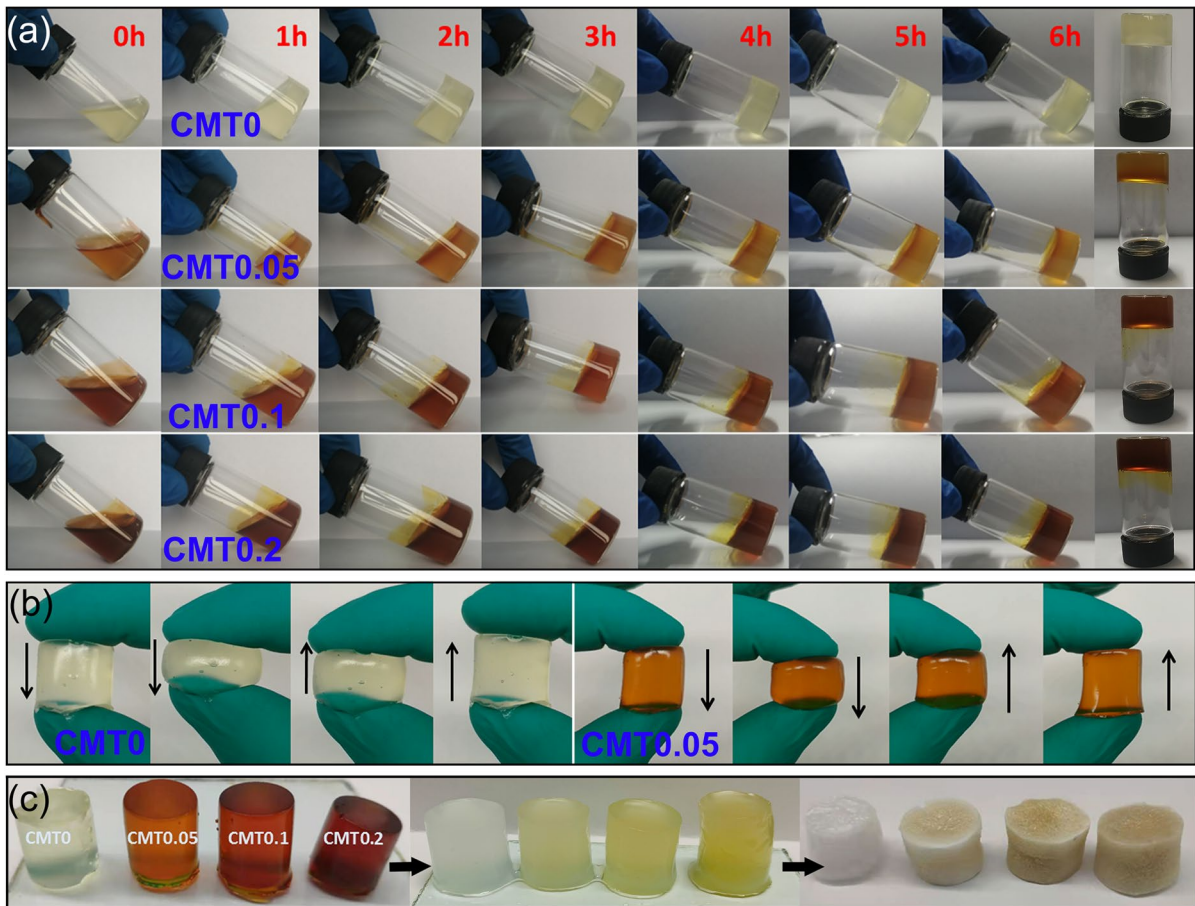
Fig. 1 **a** The gelation of CMT hydrogels over time; **b** Compression of CMT0 and CMT0.05 hydrogels; **c** The appearance of the CMT hydrogels before and after dialysis, and the CMT porous materials

found to be cross-linked in an irregular pattern. The outer shell of the porous material, akin to a "protective film," effectively impedes the occlusion of the internal pores during surface coating modification. This observation was further corroborated by analyzing the images in Fig. 2i–l. Interestingly, for PTBA-coated PCMT specimens, the internal pore structures remained unchanged, retaining their original three-dimensional configuration. However, the previously smooth surface of PCMT became rough, thereby facilitating the formation of a hydrophobic surface.

It is noteworthy that the pore size of the CMT material was determined to be more than 100 μm, which exceeds the measurable range of BET. Therefore, we conducted statistical analysis on the pore size distribution of the material. The data presented in Fig. 3 indicate that the addition of

tannin ruptures the previously uniform pore size distribution of CMT0, causing a relatively greater proportion of small-sized pores. However, the pore size distribution is influenced by the content of tannin added to the material. Specifically, with an increase in tannin concentration, the proportion of smaller pores initially increased and then decreased. Meanwhile, the density and porosity of the materials are been found in Fig. 4a. With the increase of tannin content, the density first decreases and then increases. The porosity exhibits an initial increase, followed by a decrease, with the highest porosity recorded in CMT0.1, in agreement with the outcome of the statistical analysis. The extent of tannin-induced changes in the pore structure of the porous material is limited, indicating that the oil-absorption capacity
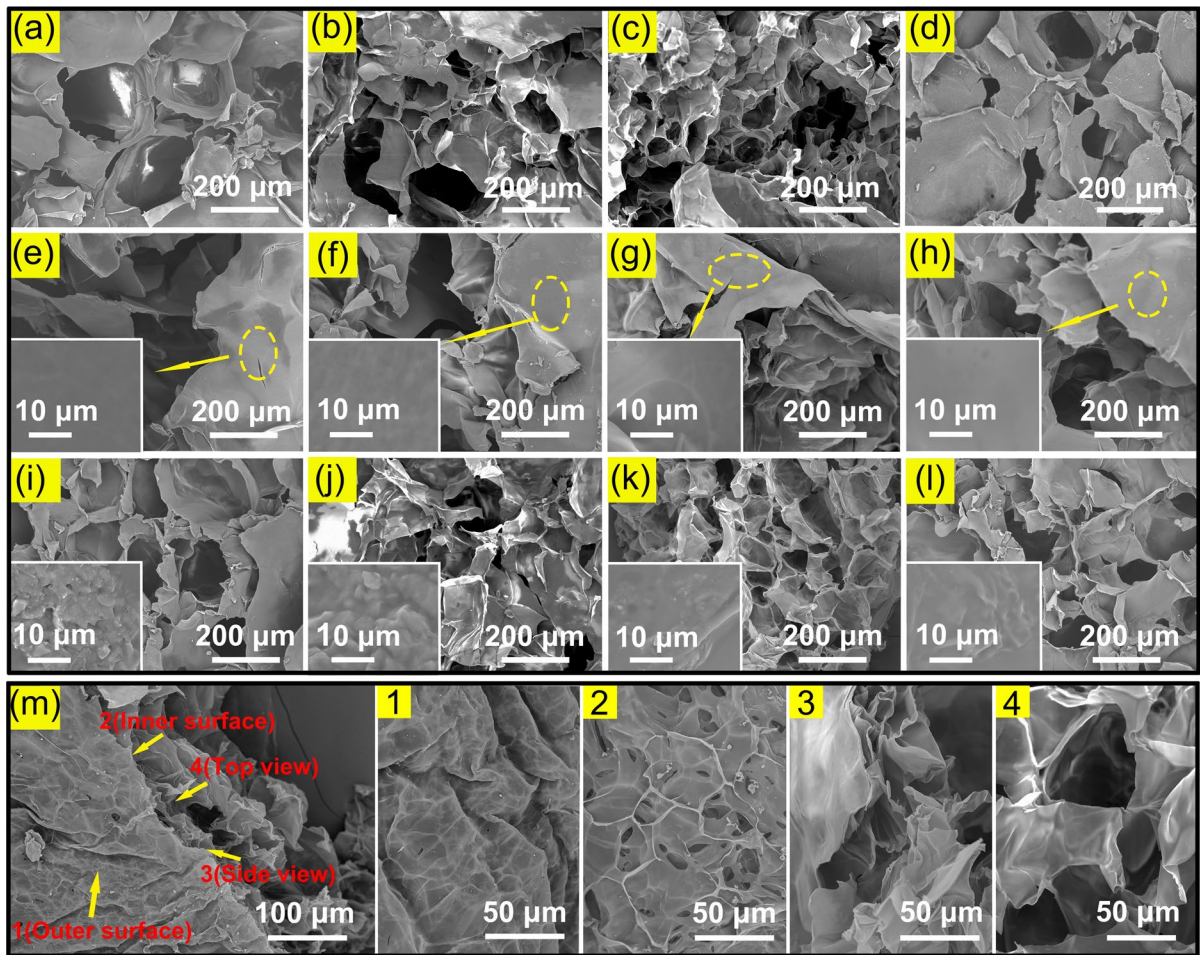
Fig. 2 The SEM images of the bulk of the porous materials: **a** CMT0, **b** CMT0.05, **c** PCMT0.1 and **d** CMT0.2; The SEM images of the surface of the porous materials: **e** CMT0, **f** CMT0.05, **g** PCMT0.1 and **h** CMT0.2; The SEM images of bulk and surface of **i** PCMT0, **j** PCMT0.05, **k** PCMT0.1 and **l** PCMT0.2; **m** the SEM images of PCMT0.1 at different directions: 1 is outer surface, 2 is an inner surface, 3 is a side view, and 4 is a top view

of the material may be attributed to its pore size distribution.

In the FTIR spectra of PTBA and porous materials, as depicted in Fig. 4b, the absorbance in the spectral range of 3200–3700 cm^{-1} corresponds to the characteristic vibration of the O–H bond present in cellulose. Notably, in the FTIR spectrum of PTBA, discernable characteristic absorptions of tertbutyl at 1363 cm^{-1} and 1391 cm^{-1} were found (Gao et al. 2011). Interestingly, the stretching vibration of C=C at 1690 cm^{-1} indicates that the C=C bond underwent depletion during gelation. Moreover, characteristic peaks of cellulose, PTBA,

and tannin were detected in the FTIR spectra of PCMT. Specifically, the FTIR spectra featured the vibration absorption of the C=O of PTBA at 1727 cm^{-1}, the bending vibration of C–O on PTBA at 1151 cm^{-1} (Wu et al. 2019), and the absorption of p-disubstituted and m-disubstituted on the benzene ring of tannin at 846 cm^{-1} and 752 cm^{-1} (Yang et al. 2019).

Thermal stability represents a crucial characteristic for materials that must withstand harsh environments. As demonstrated in the TG results (Fig. 4c, d), the weight of the materials remained unchanged at temperatures ranging from 0 to 100 °C. The tannin
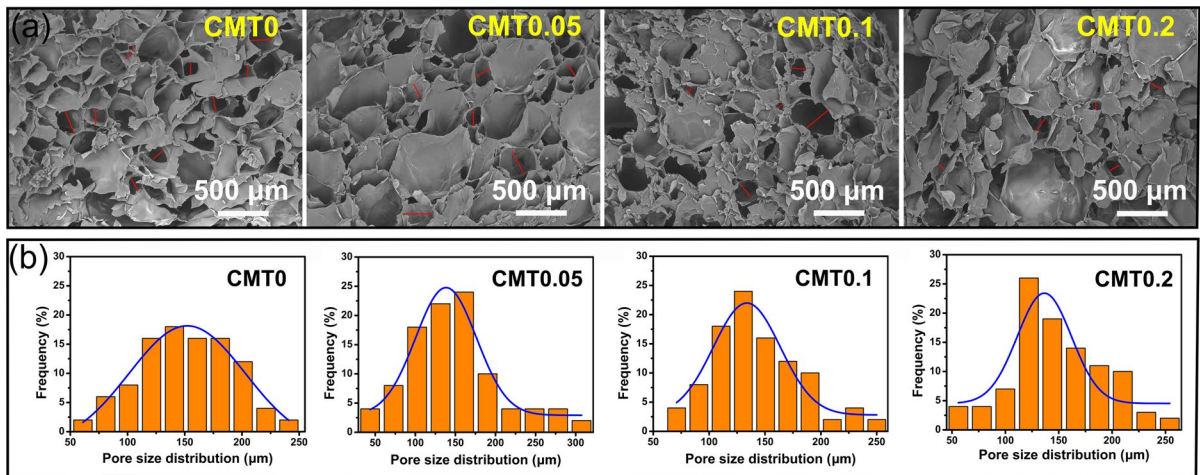
Fig. 3 a The SEM images of CMT; b The pore size distribution of CMT

Fig. 4 a The density and porosity of CMT; b The FTIR spectra of the materials; c Thermograms of cellulose, tannin, PTBA, CMT0 and PCMT0; d Thermograms of CMT0 and PCMT
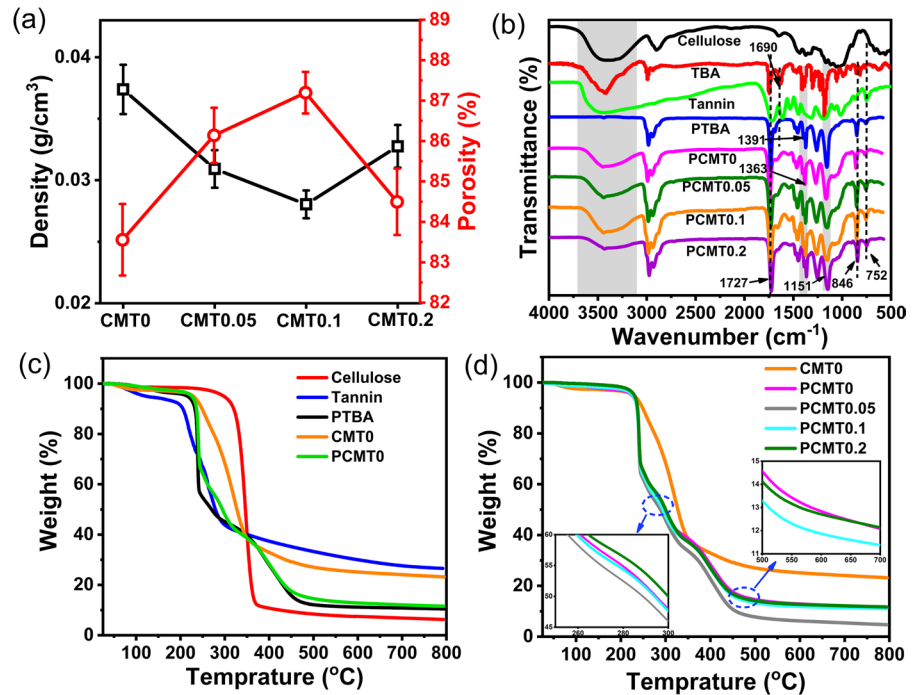
adsorbed water was observed to be lost between 100 and 200 °C, while PTBA exhibited the onset of decomposition at approximately 220 °C. This was marked by a sharp decline in weight as evidenced by the TG curves. Interestingly, a narrow temperature range was identified whereby almost 40% of weight loss occurred. Subsequently, another weight loss region was observed between 400 and 450 °C,

whereby weight loss decreased from 40 to 20%. For tannin, the dehydration process was observed to occur slightly above 100 °C. In addition, a significant weight loss of approximately 60% was noted between 220 and 300 °C, followed by a gradual weight loss above 300 °C, leaving a residual of 25%. It is noteworthy to mention that pure cellulose decomposition transpired around 360 °C, which corroborates prior findings.

The decomposition of CMT0 commenced at around 250 °C and exceeded the curve of cellulose at 350 °C. This result is interesting as CMT0 does not contain tannin, yet its residual was found to be similar to that of tannin. It is important to note that both the tannin and PTBA residues were greater than that of cellulose after 600 °C, indicating that cellulose is less thermally stable than the former two. Furthermore, the results suggest that PCMT may augment the thermal stability of cellulose materials. This is demonstrated by the fact that the decomposition curve of PCMT0 aligns with that of PTBA across the entire temperature range. Finally, it should be noted that an increase in tannin contents slightly increased the thermostability of the materials above 300 °C, as showen in Fig. 4d.

Surface wettability and oil absorption properties

The analysis of contact angles is important in discerning the surface wettability of porous materials. Initially, the CMT demonstrated strong hydrophilicity, owing to the abundance of hydroxyl groups present in cellulose (Fig. 5a). It facilitated the rapid diffusion and absorption of water droplets, which were completely absorbed within 4 s. Consequently, the contact angles ranged from 0° to 20°. Notably, the CMT also exhibited lipophilic properties, with oil droplets effortlessly spreading across the surface of the materials (Fig. 5b).

In contrast, the modified PCMT was characterized by a distinct hydrophobicity, which could be attributed to the presence of PTBA hydrophobic modifier coating the material's surface. PTBA, a product of the polymerization of multiple TBA, riches in tertbutyl groups that behave like "brooms". These tertbutyl groups exhibit large steric hindrance and hydrophobic characteristics, which in turn, constitute a hydrophobic surface with low surface energy. Thus, PTBA serves as an effective hydrophobic modifier that impedes the penetration of water into the porous structure of PCMT and effectively blocks external water (Fig. 6a).

Subsequent tests demonstrated that the contact angles of water on PCMT surface ranged between 106.5° and 121.5° (Fig. 6b), which is comparatively lower than that reported in literature (> 140°) (Xie et al. 2021; Yu et al. 2020; Zhou et al. 2019). However, this lower contact angle did not affect the oil–water separation efficiency, hydrophobic stability and environmental adaptability of PCMT.

Fig. 5 **a** Contact angle of water on CMT surfaces and PCMT surfaces; **b** Wetting behaviours of CMT
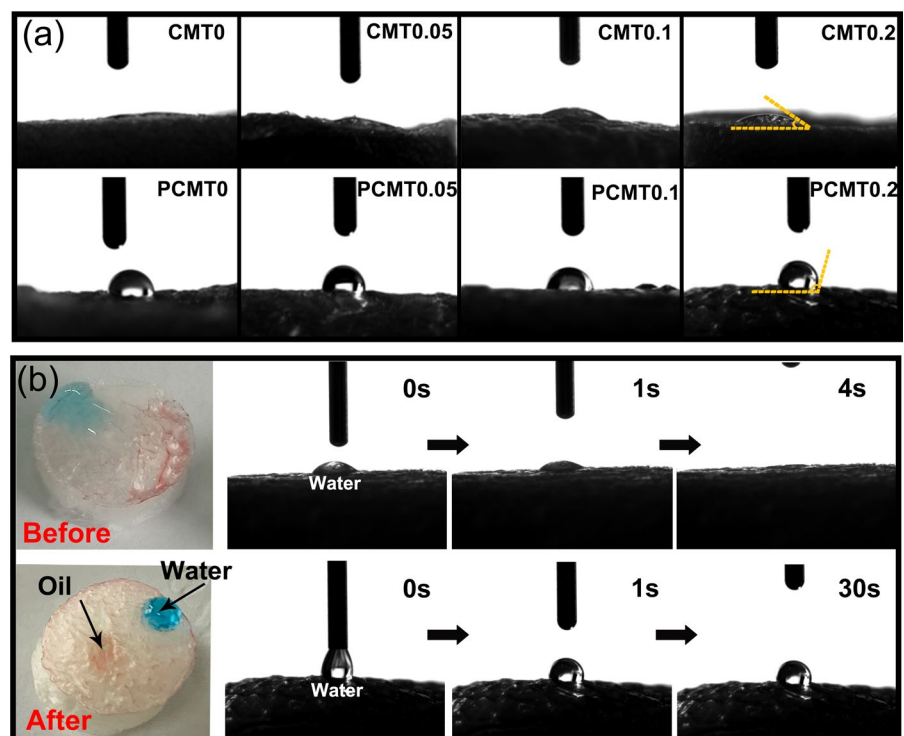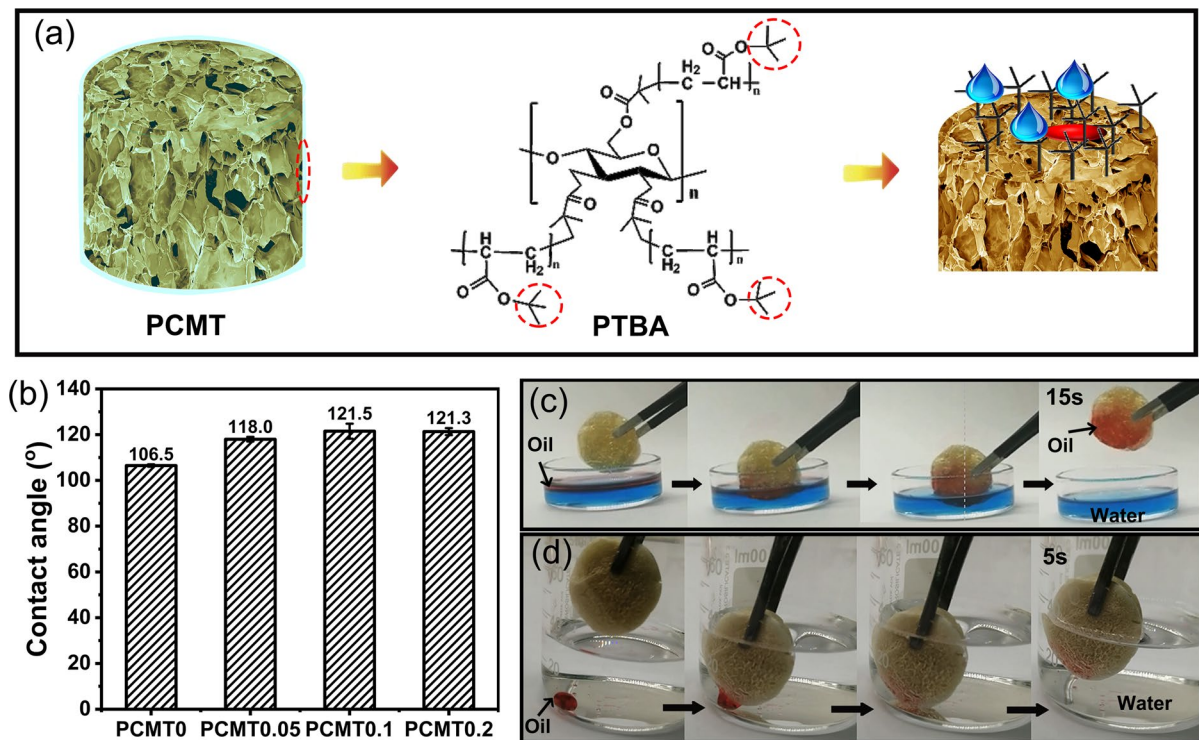
Fig. 6 **a** Illustration of the chemical structure exposed on the PCMT surface; **b** Contact angle of water on the PCMT surface; **c** Absorption of n-hexane in the PCMT; **d** Absorption of dichloromethane in the PCMT under water

Visual inspections were conducted to evaluate the ability of PCMT to absorb two organic solvents, one lighter and one heavier than water, respectively (Fig. 6c, d). The results indicated that PCMT could selectively absorb the oil phase from the water phase, thus, highlighting its exceptional hydrophobicity and lipophilicity.

The oil absorption selectivity of PCMT was demonstrated through the simulation of oil pollution using four organic reagents. The selected reagents, namely petroleum ether, n-hexane, toluene, and dichloromethane, serve as representatives of heavy oil, light oil, alkane, aromatic, and halogen oils, respectively. These reagents exhibit low viscosity. The adsorption capacity-time diagram of PCMT for n-hexane model oils is depicted in Fig. 7a, which reveals that the absorption capacity of PCMT for n-hexane increases rapidly within the first ten seconds, followed by a slow increase, eventually reaching equilibrium in one minute. This phenomenon can be attributed to the initial stage of adsorption, where PCMT contains a substantial number of pore volumes, enabling it to accommodate more oil phases, thereby accelerating its adsorption rate. However, as the oil adsorption capacity increases, the remaining unoccupied pore volume in PCMT decreases, leading to a reduction in its adsorption rate, eventually reaching adsorption saturation. The adsorption behavior of PCMT to oil follows the second-order kinetic model, with a high correlation coefficient (Fig. 7b).

To examine the oil absorption capacity of PCMT, one-minute absorption tests were conducted on the four organic liquids, as shown in Fig. 7c. The results indicate that PCMT can generally absorb 4–8 times its weight. Although the absorption capacity of PCMT is not remarkable compared to other materials reported in the literature, the adsorption of PCMT to the four oils displayed differences. There is no discernible trend with the absorptive capacities of the oils as the tannin content increases in PCMT. For instance, the polarities of petroleum ether and n-hexane are similar, but the absorptive capacity of the different PCMT materials varies. PCMT0 (petroleum ether 6.27 g/g)
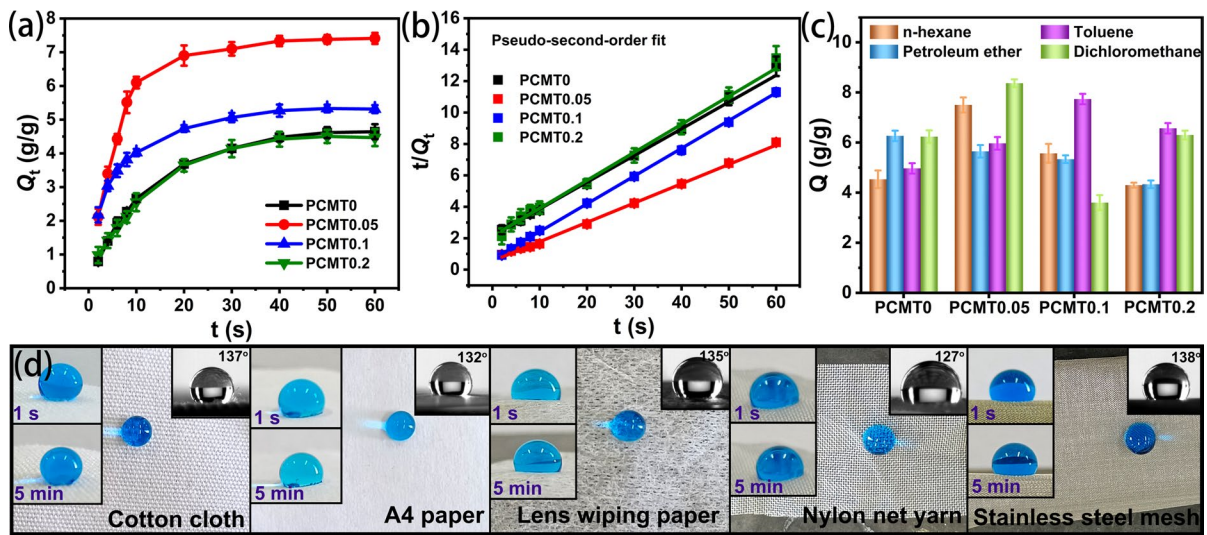
Fig. 7 **a** Adsorption capacities of PCMT for n-hexane with time; **b** The pseudo-second-order kinetic model fitting; **c** Adsorption capacities of PCMT for four oils; **d** Contact angles of water on PTBA coated surfaces

and PCMT0.05 (n-hexane 7.51 g/g) exhibit the maximum absorption. For toluene, PCMT0.1 showed the highest absorption (7.73 g/g). For high-density organic liquids like dichloromethane, PCMT0.05 had the best absorption capacity (8.37 g/g).

Many variables are known to impact the absorptive capacity, including the porous size and the density of oil (Gao et al. 2018), among other factors. Therefore, the viscosity and density of the four oils under investigation have been collated and presented in Table S1, as supplementary data. It is noteworthy that dichloromethane, followed by toluene, has the highest viscosity and density, while n-hexane and petroleum ether share similar properties. Typically, materials designed to absorb oil exhibit a high absorptive capacity for heavy oil, characterized by high density and viscosity (e.g., dichloromethane), and a low absorptive capacity for light oil, with low viscosity and density (Laitinen et al. 2017; Li et al. 2019; Xiong et al. 2018). Nonetheless, our findings contradict this trend. Specifically, only PCMT0.05 demonstrated the highest absorptive capacity for dichloromethane, while PCMT0.1 exhibited the lowest. The absorptive capacity of other materials for these four organic liquids also varies, and we failed to establish any general trend. It is our speculation that physicochemical properties of PCMT, such as its wetting, pore size, and pore volume, also exert

influence on its absorptive capacity, in addition to oil density. Pore volume and pore size of materials directly impact oil passing and filling, hence affecting its absorptive capacity. Greater pore volume translates into a larger oil absorptive capacity. However, if the pore size of the material is excessively large, the surface tension of the liquid might fail to hold the oil weight, thereby limiting the oil absorptive capacity. These findings indicate that the pore structure of porous materials is central to determining their oil adsorption capacity. In the present study, PCMT0.05, on average, demonstrated the highest absorption capacity among the four materials.

To demonstrate the applicability of coating PTBA as a universal technique for surface modification, we proceeded to coat cotton cloth, A4 paper, stainless steel mesh, lens wiping paper, and nylon net yarn using PTBA (Fig. 7d). Following the PTBA coating process, the contact angles on the various surfaces, including cotton cloth, A4 paper, stainless steel mesh, lens wiping paper, and nylon net yarn, spanned from 127° to 138°. These surfaces may be categorized into three groups based on their respective chemical compositions. Namely, cotton cloth, A4 paper, and lens wiping paper predominantly comprise cellulose, while steel mesh and nylon fabrics consist of metal and polymer, respectively. It is noteworthy that the contact angle on nylon fabric exhibits the lowest

value, reaching a mere 127°. Meanwhile, the contact angles on lens paper, cotton, and metal surfaces are strikingly comparable, falling within a range of 135° to 137°. The contact angle on A4 paper measures at 132°. Notably, water droplets maintained their form on these surfaces for up to five minutes. The water contact angles of these materials surpass that of the PCMT. It could be due to the irregular surface of CMT prepared through freeze-drying. Nonetheless, two factors affect surface properties: roughness and surface chemistry. In this scenario, all fabrics underwent PTBA modification, thereby presenting identical chemical properties on their surfaces. Consequently, the disparity in contact angle must be attributed to surface roughness.

Mechanical properties

For porous materials, the introduction of tannin grants not only a transformation of porosity, but also a reconfiguration of the mechanical characteristics (Fig. 8). PCMT, in particular, displays a stress–strain hysteresis loop even when subjected to a strain of 30% (Fig. 8a, b). Intriguingly, the compressive curves manifest themselves in two linear sections, signaling the presence of dual elastic structures within the materials. This phenomenon is especially pronounced in curves subjected to a strain of 80%. As a concrete example, in Fig. 8a, the breaking point emerges at a strain of 53%, effectively separating two slopes (namely, Young's modulus). Initially, a weak network of porous material is subjected to external forces and undergoes compression. Subsequently, a more robust network of materials experiences compression. This outcome is in accordance with the morphology of the internal pore structure, which varies in size as showed in the SEM images in Fig. 3. In Fig. 8c, d, the compressive strength of PCMT increases with escalating tannin content, with PCMT0.2 (290.3 kPa) registering the highest strength, at approximately 3.8 times greater than that of PCMT0. In sum, these four porous materials can withstand over 7000 times their weight. In addition, the sound of internal aperture fracture was not heard when the porous material was subjected to 500 g weight, and the SEM image of the porous material after load-bearing did not change (Fig. 8c), showing a complete three-dimensional
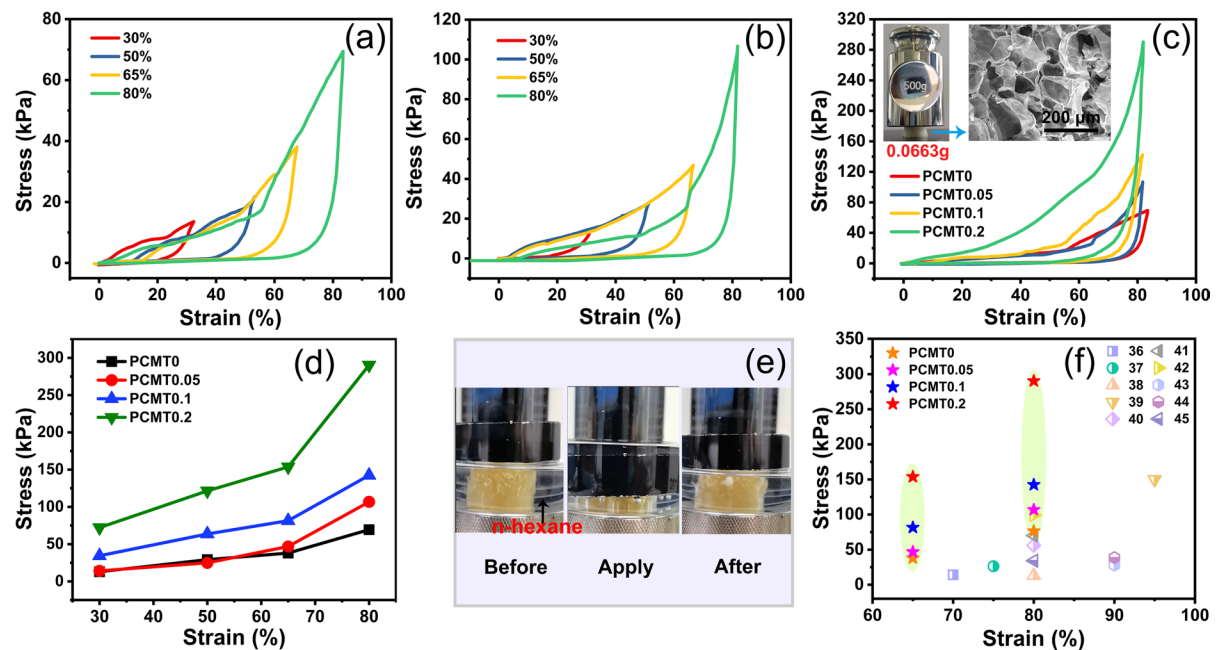
Fig. 8 Stress–strain hysteresis loops of **a** PCMT0 and **b** PCMT0.05; **c** stress–strain hysteresis loops of the PCMT with 80% strain; **d** Stress–strain hysteresis loops of the PCMT; **e** Compression of porous materials in n-hexane. **f** Comparison of the mechanical property of different cellulose materials

cross-networking structure and verified their remarkable mechanical properties.

In Fig. 8e, we have documented the process of compressing PCMT in n-hexane. Despite the observation of a hysteresis loop during compression, the PCMT was able to recover its original form. It is probable that the internal structure of the porous materials may have suffered partial destruction during compression, though such destruction did not affect the next absorption cycle. This demonstrates the excellent resilience of the PCMT, as oil can be effortlessly retrieved through simple extrusion, yielding a straightforward oil recovery protocol. Moreover, the mechanical properties of PCMT0.05, PCMT0.1, and PCMT0.2 surpass those of many

cellulose-based materials with an 80% strain near (as shown in Fig. 8f and supplementary data Table S2).

Environmental suitability and recyclability

In an effort to emulate the intricate conditions of oily wastewater in a genuine setting, the durability and resistance of PCMT porous materials to complex environments were assessed. The specimen PCMT0.1 served as an example, as its hydrophobic stability and n-hexane absorption capabilities were put to the test in a variety of conditions. These included stirring, different temperatures, distinct pH values, ultraviolet irradiation, and surface peeling.
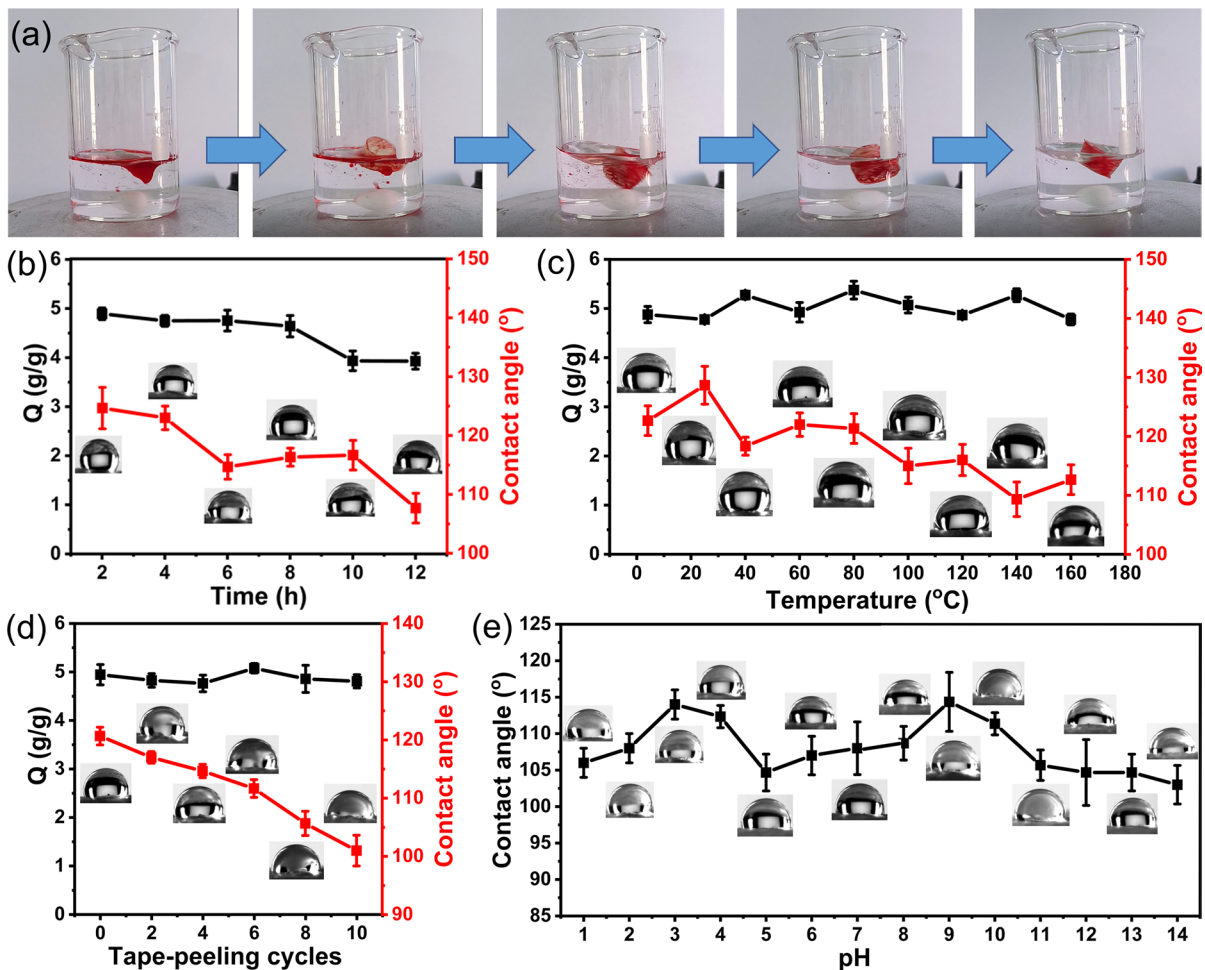
Fig. 9 a The absorption process of n-hexane under vigorous stirring. Contact angles and absorption capacities in different environments: b irradiation with a 250 W UV lamp; c different temperatures; d tape-peeling; e pH

As demonstrated in Fig. 9a, the PCMT porous material proved adept at entirely absorbing oil from a beaker in vigorous stirring. Meanwhile, Fig. 9b shows the material's surface wettability under ultraviolet irradiation. Though the contact angle of water and absorption of n-hexane underwent slight decreases with the passage of time under UV irradiation, both remained within acceptable parameters. However, after a duration of 12 h of irradiation, the water contact angle and oil absorptive capacity declined to 107.5° and 3.93 g/g, respectively, as a result of surface degradation attributable to the PTBA coating.

On the other hand, the material exhibited impressive resistance to high temperatures (Fig. 9c). While the water contact angles gradually declined with rising temperatures, they remained above 110°, with the absorptive capacity of n-hexane undergoing little change. Even when subjected to surface peeling using tape, the porous materials maintained their hydrophobicity, with their water contact angle remaining above 100° following 10 peeling attempts (Fig. 9d). This was largely due to the PTBA coating being stripped away through peeling, without affecting the internal pore structure of the material.

Further, pH was identified as a crucial external factor affecting absorption. Figure 9e illustrates the varying contact angles of water at different pH values. Despite slight variations in the formation of water droplets on the material's surface, the contact angles remained above 100° across a broad pH range of 1 to 14, indicating that the porous materials possessed excellent pH resistance and hydrophobicity across acidic and alkaline environments. Compared to other materials (Table 1), PCMT proved more adaptable to a wider range of environments, retaining exceptional hydrophobic stability even in the harshest of conditions. In clusion, PCMT porous materials demonstrated exceptional adaptability to environmental changes, resistivity to corrosion, and remarkable durability.

The reusability of porous materials in the treatment of oil spills in the environment is of importance, and it constitutes a critical element in the assessment of the regenerative potential of an adsorbent. In Fig. 10a–d, the absorption capacity of PCMT, concerning toluene, dichloromethane, petroleum ether, and n-hexane, respectively, underwent changes across ten cycles. Notably, the PCMT exhibited relatively commendable reusability. Nevertheless, after the second cycle, the oil absorption capacities of the PCMT notably declined due to the destruction of its pores during the extrusion process, thereby reducing its effective pore volume and consequently affecting its absorption potential during the next cycle. However, between the second and tenth absorption cycles, the oil absorption capacities of the PCMT remained nearly constant or slightly decreased.

Regarding PCMT0, the oil absorptive capacity followed the order: petroleum ether > toluene > dichloromethane > n-hexane. For PCMT0.05, dichloromethane > petroleum ether > n-hexane > toluene, and for PCMT0.1, toluene > petroleum ether > dichloromethane > n-hexane. Finally, for PCMT0.2, it was dichloromethane > n-hexane > toluene > petroleum ether.

Table 1 Comparison of environmental adaptability of cellulose-based oil absorbing materials

Materials	Environmental adaptability	References
3D cellulose-based aerogel	pH (11–13); Temperature (50–60 °C)	Zhao et al. (2017)
Cellulose acetate monolith	pH (1–14); Temperature (0–70 °C); Strong stirring	Zhang (2020)
Sisal leaves-carbon fiber aerogel	pH (2–12); HCl (1 M), NaOH (1 M), NaCl (1 M), Na_2CO_3 (1 M) and H_2O for 12 h	Liu et al. (2018)
Modification-cellulose nanofibril/silica fiber/Fe_3O_4	pH (1, 3, 7, 12, 13.5)	Mi et al. (2020)
TiO_2-assembled Biomass carbon aerogel	pH (2–13)	Yuan et al. (2018)
Bacterial cellulose/silica aerogels	Temperature (− 200, 0, 100, 200, 300 °C)	He et al. (2018)
Octadecylamine-modified silk fibroin fibers	pH (3–11)	Patowary et al. (2016)
Raw cotton fiber-cellulose aerogel	pH (1–13); NaCl (1 M)	Wang and Liu (2019)
PCMT	Vigorous stirring (1300 rpm/min); pH (1–14); Temperature (4–160 °C); Ultraviolet irradiation (8 h); Tape peeling (10 times)	This work
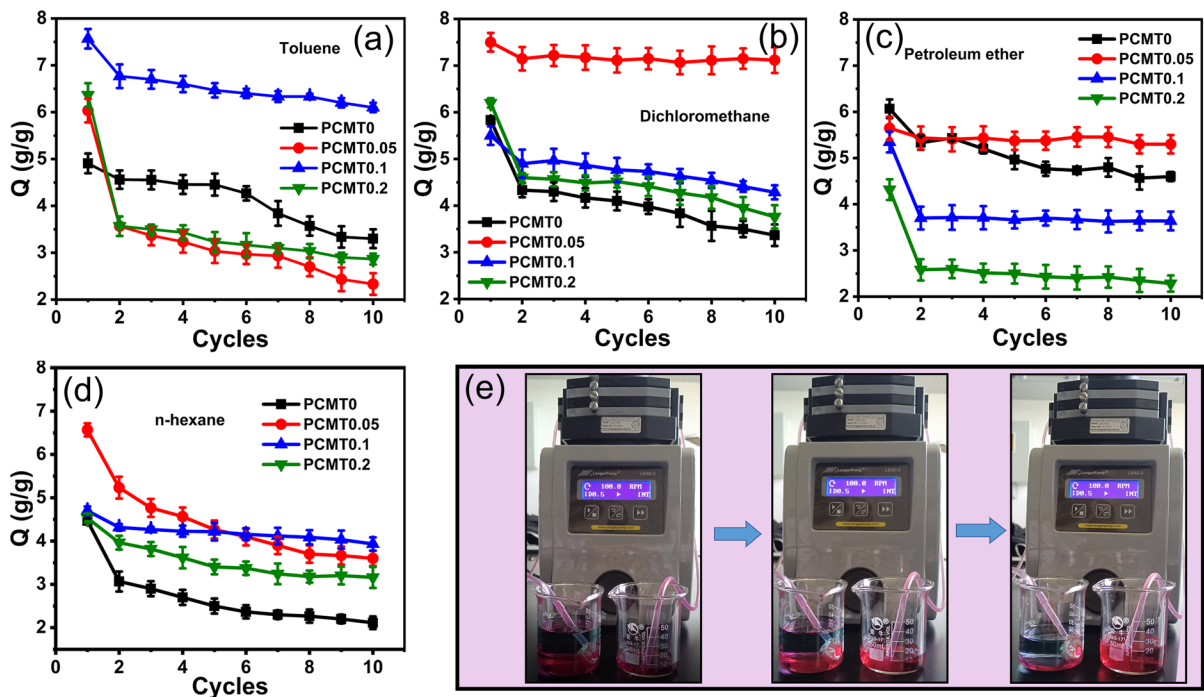
Fig. 10 Oil absorption cycles of **a** PCMT0, **b** PCMT0.05, **c** PCMT0.1 and **d** PCMT0.2; **e** continuous separating n-hexane from water

To demonstrate the continuous absorption performance of PCMT for oil, we employed a peristaltic pump to keep pumping oil into the system. Figure 10e shows that in the oil–water mixture in the left beaker, the red n-hexane was consistently separated from the blue water, which was not pumped away. This finding successfully highlights the superior performance of PCMT in terms of continuous oil absorption.

Conclusions

In this study, we have successfully prepared four porous PCMTs that possess remarkable environmental adaptability and compressive strength. This was achieved through a simple and cost-effective method that involves MBA crosslinking, freeze-drying, and surface coating.

The internal pore structure and hydrophobic surface properties of the PCMTs contribute to their excellent performance in various complex environments. They demonstrate remarkable hydrophobicity, oil–water separation, compressive ability, and resistance to harsh conditions such as UV irradiation, strong stirring, high temperatures, wide pH values, and tape peeling. In fact, these PCMTs exhibit an excellent ability to withstand 7000 times their own weight. Furthermore, their hydrophobicity remains intact under extreme environmental conditions. This is a proof to their remarkable durability and resilience. The absorption capacities of the PCMTs for different oils, such as petroleum ether, toluene, dichloromethane, and n-hexane, vary due to the difference in pore sizes. Moreover, the absorption capacity of the PCMTs decreases in the second compression cycle due to the changes in pore sizes and mechanical strength. Nevertheless, the PCMTs continue to maintain their outstanding performance even after the second compression cycle. Overall, our study demonstrates the promising potential of these PCMTs in various applications, such as environmental remediation and separation processes, owing to their excellent performance and cost-effective synthesis method.

Declarations

References

ben Hammouda S, Chen Z, An C, Lee K (2021) Recent advances in developing cellulosic sorbent materials for oil spill cleanup: a state-of-the-art review. J Clean Prod 311:127630. https://doi.org/10.1016/j.jclepro.2021.127630

Cao J, Wang Z, Yang X, Tu J, Wu R, Wang W (2018) Green synthesis of amphipathic graphene aerogel constructed by using the framework of polymer-surfactant complex for water remediation. Appl Surf Sci 444:399–406. https://doi.org/10.1016/j.apsusc.2018.02.282

Chen C, Weng D, Mahmood A, Chen S, Wang J (2019) Separation mechanism and construction of surfaces with special wettability for oil/water separation. ACS Appl Mater Interfaces 11:11006–11027. https://doi.org/10.1021/acsami.9b01293

Cheng Z et al (2020) Scalable and robust bacterial cellulose carbon aerogels as reusable absorbents for high-efficiency oil/water separation. ACS Appl Bio Mater 3:7483–7491. https://doi.org/10.1021/acsabm.0c00708

Cho E-C et al (2017) Robust multifunctional superhydrophobic coatings with enhanced water/oil separation, self-cleaning, anti-corrosion, and anti-biological adhesion. Chem Eng J 314:347–357. https://doi.org/10.1016/j.cej.2016.11.145

Dai C et al (2020) Assembly of ultralight dual network graphene aerogel with applications for selective oil absorption. Langmuir 36:13698–13707. https://doi.org/10.1021/acs.langmuir.0c02664

Das I, De G (2015) Zirconia based superhydrophobic coatings on cotton fabrics exhibiting excellent durability for versatile use. Sci Rep 5:18503. https://doi.org/10.1038/srep18503

Davis KA, Matyjaszewski K (2000) Atom transfer radical polymerization of tert-butyl acrylate and preparation of block copolymers. Macromolecules 33:4039–4047. https://doi.org/10.1021/ma991826s

Fei Y et al (2022) In situ construction strategy for three-dimensional Janus cellulose aerogel with highly efficient oil–water separation performance: from hydrophobicity to asymmetric wettability. Green Chem 24:7074–7081. https://doi.org/10.1039/d2gc02275c

Fu J, He C, Wang S, Chen Y (2018) A thermally stable and hydrophobic composite aerogel made from cellulose nanofibril aerogel impregnated with silica particles. J Mater Sci 53:7072–7082. https://doi.org/10.1007/s10853-018-2034-9

Gao J, Li X, Lu Q, Li Y, Ma D, Yang W (2011) Synthesis and characterization of poly(methyl methacrylate-butyl acrylate) by using glow-discharge electrolysis plasma. Polym Bull 68:37–51. https://doi.org/10.1007/s00289-011-0517-9

Gao R et al (2018) Mussel adhesive-inspired design of superhy-drophobic nanofibrillated cellulose aerogels for oil/water separation. ACS Sustain Chem Eng 6:9047–9055. https://doi.org/10.1021/acssuschemeng.8b01397

Hai J, Bai B, Ding C, Wang H, Suo Y (2018) Removal of oil from water surface by novel composite NSM-g-P(MMA-co-BA) super oil-absorption resin. Polym Compos 39:1051–1063. https://doi.org/10.1002/pc.24032

He J, Zhao H, Li X, Su D, Zhang F, Ji H, Liu R (2018) Super-elastic and superhydrophobic bacterial cellulose/silica aerogels with hierarchical cellular structure for oil absorption and recovery. J Hazard Mater 346:199–207. https://doi.org/10.1016/j.jhazmat.2017.12.045

Klein JW, Lamps J-P, Gnanou Y, Rempp P (1991) Synthesis and characterization of block copolymers containing poly(tert.butyl acrylate) blocks. Polymer 32:2278–2282. https://doi.org/10.1016/0032-3861(91)90059-R

Laitinen O, Suopajarvi T, Osterberg M, Liimatainen H (2017) Hydrophobic, superabsorbing aerogels from choline chloride-based deep eutectic solvent pretreated and silylated

cellulose nanofibrils for selective oil removal. ACS Appl Mater Interfaces 9:25029–25037. https://doi.org/10.1021/acsami.7b06304

Lang D et al (2021) DMAEMA-grafted cellulose as an imprinted adsorbent for the selective adsorption of 4-nitrophenol. Cellulose 28:6481–6498. https://doi.org/10.1007/s10570-021-03920-9

Li Z, Zhong L, Zhang T, Qiu F, Yue X, Yang D (2019) Sustainable, flexible, and superhydrophobic functionalized cellulose aerogel for selective and versatile oil/water separation. ACS Sustain Chem Eng 7:9984–9994. https://doi.org/10.1021/acssuschemeng.9b01122

Liu H, Geng B, Chen Y, Wang H (2016) Review on the aerogel-type oil sorbents derived from nanocellulose. ACS Sustainable Chem Eng 5:49–66. https://doi.org/10.1021/acssuschemeng.6b02301

Liu Y, Peng Y, Zhang T, Qiu F, Yuan D (2018) Superhydrophobic, ultralight and flexible biomass carbon aerogels derived from sisal fibers for highly efficient oil–water separation. Cellulose 25:3067–3078. https://doi.org/10.1007/s10570-018-1774-7

Liu L, Pan Y, Bhushan B, Zhao X (2019) Mechanochemical robust, magnetic-driven, superhydrophobic 3D porous materials for contaminated oil recovery. J Colloid Interface Sci 538:25–33. https://doi.org/10.1016/j.jcis.2018.11.066

Lorevice MV, Mendonça EO, Orra NM, Borges AC, Gouveia RF (2020) Porous cellulose nanofibril–natural rubber latex composite foams for oil and organic solvent absorption. ACS Appl Nano Mater 3:10954–10965. https://doi.org/10.1021/acsanm.0c02203

Mi H-Y, Li H, Jing X, Zhang Q, Feng P-Y, He P, Liu Y (2020) Superhydrophobic cellulose nanofibril/silica fiber/Fe$_3$O$_4$ nanocomposite aerogel for magnetically driven selective oil absorption. Cellulose 27:8909–8922. https://doi.org/10.1007/s10570-020-03397-y

Nie X, Lv P, Stanley SL, Wang D, Wu S, Wei Q (2019) Ultralight nanocomposite aerogels with interpenetrating network structure of bacterial cellulose for oil absorption. J Appl Polym Sci 136:48000. https://doi.org/10.1002/app.48000

Patoway M, Pathak K, Ananthakrishnan R (2016) Robust superhydrophobic and oleophilic silk fibers for selective removal of oil from water surfaces. RSC Adv 6:73660–73667. https://doi.org/10.1039/c6ra14723b

Peng B, Yao Z, Wang X, Crombeen M, Sweeney DG, Tam KC (2020) Cellulose-based materials in wastewater treatment of petroleum industry. Green Energy Environ 5:37–49. https://doi.org/10.1016/j.gee.2019.09.003

Qin X et al (2019) Superelastic and durable hierarchical porous thermoplastic polyurethane monolith with excellent hydrophobicity for highly efficient oil/water separation. Ind Eng Chem Res 58:20291–20299. https://doi.org/10.1021/acs.iecr.9b03717

Tai MH, Mohan BC, Yao Z, Wang CH (2022) Superhydrophobic leached carbon Black/Poly(vinyl) alcohol aerogel for selective removal of oils and organic compounds from water. Chemosphere 286:131520. https://doi.org/10.1016/j.chemosphere.2021.131520

Wang J, Liu S (2019) Remodeling of raw cotton fiber into flexible, squeezing-resistant macroporous cellulose aerogel with high oil retention capability for oil/water separation. Sep Purif Technol 221:303–310. https://doi.org/10.1016/j.seppur.2019.03.097

Wu X et al (2019) Hydrophobic poly(tert-butyl acrylate) photonic crystals towards robust energy-saving performance. Angew Chem Int Ed 58:13556–13564. https://doi.org/10.1002/anie.201907464

Wu Z et al (2021) One-pot fabrication of hydrophilic-oleophobic cellulose nanofiber-silane composite aerogels for selectively absorbing water from oil–water mixtures. Cellulose 28:1443–1453. https://doi.org/10.1007/s10570-020-03610-y

Xie X, Zheng Z, Wang X, Lee Kaplan D (2021) Low-density silk nanofibrous aerogels: fabrication and applications in air filtration and oil/water purification. ACS Nano 15:1048–1058. https://doi.org/10.1021/acsnano.0c07896

Xiong Q, Bai Q, Li C, Lei H, Liu C, Shen Y, Uyama H (2018) Cost-effective, highly selective and environmentally friendly superhydrophobic absorbent from cigarette filters for oil spillage clean up. Polymers (Basel) 10:1101. https://doi.org/10.3390/polym10101101

Yang B et al (2019) Evaluation of activated carbon synthesized by one-stage and two-stage co-pyrolysis from sludge and coconut shell. Ecotox Environ Safe 170:722–731. https://doi.org/10.1016/j.ecoenv.2018.11.130

Yin T, Zhang X, Liu X, Wang C (2017) Resource recovery of *Eichhornia crassipes* as oil superabsorbent. Mar Pollut Bull 118:267–274. https://doi.org/10.1016/j.marpolbul.2017.01.064

Yu Y, Shi X, Liu L, Yao J (2020) Highly compressible and durable superhydrophobic cellulose aerogels for oil/water emulsion separation with high flux. J Mater Sci 56:2763–2776. https://doi.org/10.1007/s10853-020-05441-5

Yuan D, Zhang T, Guo Q, Qiu F, Yang D, Ou Z (2018) Superhydrophobic hierarchical biomass carbon aerogel assembled with TiO$_2$ nanorods for selective immiscible oil/water mixture and emulsion separation. Ind Eng Chem Res 57:14758–14766. https://doi.org/10.1021/acs.iecr.8b03661

Zhang X et al (2020) Cellulose acetate monolith with hierarchical micro/nano-porous structure showing superior hydrophobicity for oil/water separation. Carbohydr Polym 241:116361. https://doi.org/10.1016/j.carbpol.2020.116361

Zhang H, Wang J, Xu G, Xu Y, Wang F, Shen H (2021) Ultralight, hydrophobic, sustainable, cost-effective and floating kapok/microfibrillated cellulose aerogels as speedy and recyclable oil superabsorbents. J Hazard Mater 406:124758. https://doi.org/10.1016/j.jhazmat.2020.124758

Zhang F, Wang C, Mu C, Lin W (2022) A novel hydrophobic all-biomass aerogel reinforced by dialdehyde carboxymethyl cellulose for oil/organic solvent-water separation. Polymer 238:124402. https://doi.org/10.1016/j.polymer.2021.124402

Zhao L, Li L, Wang Y, Wu J, Meng G, Liu Z, Guo X (2017) Preparation and characterization of thermo- and pH dual-responsive 3D cellulose-based aerogel for oil/water separation. Appl Phys A 124:9. https://doi.org/10.1007/s00339-017-1358-7

Zhou L, Zhai S, Chen Y, Xu Z (2019) Anisotropic cellulose nanofibers/polyvinyl alcohol/graphene aerogels fabricated by directional freeze-drying as effective oil adsorbents. Polymers 11:712. https://doi.org/10.3390/polym11040712